



HAL
open science

Experimental investigations of diacetylene ice photochemistry in Titan's atmospheric conditions

Benjamin Fleury, Murthy Gudipati, Isabelle Couturier-Tamburelli

► To cite this version:

Benjamin Fleury, Murthy Gudipati, Isabelle Couturier-Tamburelli. Experimental investigations of diacetylene ice photochemistry in Titan's atmospheric conditions. *Astronomy and Astrophysics - A&A*, 2024, 684, pp.A1. 10.1051/0004-6361/202348658 . hal-04529416

HAL Id: hal-04529416

<https://hal.science/hal-04529416>

Submitted on 3 Apr 2024



HAL is a multi-disciplinary open access archive for the deposit and dissemination of scientific research documents, whether they are published or not. The documents may come from teaching and research institutions in France or abroad, or from public or private research centers.

L'archive ouverte pluridisciplinaire **HAL**, est destinée au dépôt et à la diffusion de documents scientifiques de niveau recherche, publiés ou non, émanant des établissements d'enseignement et de recherche français ou étrangers, des laboratoires publics ou privés.



Distributed under a Creative Commons Attribution 4.0 International License

Experimental investigations of diacetylene ice photochemistry in Titan's atmospheric conditions

Benjamin Fleury^{1,2} , Murthy S. Gudipati² , and Isabelle Couturier-Tamburelli³

¹ Université Paris Cité and Univ Paris Est Creteil, CNRS, LISA, 75013 Paris, France
e-mail: benjamin.fleury@lisa.ipsl.fr

² Jet Propulsion Laboratory, California Institute of Technology, 4800 Oak Grove Drive, Pasadena, CA 91109, USA

³ Aix-Marseille Université, CNRS, PIIM, UMR 7345, 13013 Marseille, France
e-mail: isabelle.couturier@univ-amu.fr

Received 17 November 2023 / Accepted 31 January 2024

ABSTRACT

Context. A large fraction of the organic species produced photochemically in the atmosphere of Titan can condense to form ice particles in the stratosphere and in the troposphere. According to various studies, diacetylene (C_4H_2) condenses below 100 km where it can be exposed to ultraviolet radiation.

Aims. We studied experimentally the photochemistry of diacetylene ice (C_4H_2) to evaluate its potential role in the lower altitude photochemistry of Titan's atmospheric ices.

Methods. C_4H_2 ice films were irradiated with near-ultraviolet (near-UV) photons ($\lambda > 300$ nm) with different UV sources to assess the impact of the wavelengths of photons on the photochemistry of C_4H_2 . The evolution of the ice's composition was monitored using spectroscopic techniques.

Results. Our results reveal that diacetylene ice is reactive through singlet-triplet absorption, similar to the photochemistry of other organic ices of Titan (such as dicyanoacetylene C_4N_2 ice) that we investigated previously. Several chemical processes occurred during the photolysis: the hydrogenation of C_4H_2 to form other C_4 hydrocarbons (vinylacetylene C_4H_4 to butane C_4H_{10}); the formation of larger and highly polymerizable hydrocarbons, such as triacetylene (C_6H_2); and the formation of an organic polymer that is stable at room temperature.

Conclusions. The nondetection of diacetylene ice in Titan's atmosphere or surface could be rationalized based on our experimental results that C_4H_2 is photochemically highly reactive in the solid phase when exposed to near-UV radiation that reaches Titan's lower altitudes and surface. C_4H_2 may be one of the key molecules promoting the chemistry in the ices and aerosols of Titan's haze layers, especially in the case of co-condensation with other organic volatiles, with which it could initiate more complex solid-phase chemistry.

Key words. astrochemistry – methods: laboratory: molecular – techniques: spectroscopic – planets and satellites: atmospheres – ultraviolet: planetary systems

1. Introduction

The complex organic chemistry initiated in Titan's thermosphere and ionosphere by solar photons and energetic particles of Saturn's magnetosphere leads to the production of many volatile organics as well as organic aerosols (Lavvas et al. 2013; Liang et al. 2007; Waite et al. 2007). The decrease in temperature from the stratosphere to the tropopause (Fulchignoni et al. 2005) allows the direct condensation of many volatiles (hydrocarbons and nitriles), thus forming ice particles or ice accreted on organic aerosols (Anderson et al. 2016; Barth 2003, 2017; de Kok et al. 2008; Frère et al. 1990; Lavvas et al. 2011; Mayo & Samuelson 2005; Raulin & Owen 2002; Sagan & Reid Thompson 1984; Samuelson & Mayo 1991; Samuelson et al. 1997).

Gas molecules and organic hazes in Titan's atmosphere significantly attenuate high-energy photons. As a result, only longer-wavelength photons make it through the stratosphere and the troposphere and eventually to the surface of Titan. Vuitton et al. (2019) model the flux of photons from 1.5 to 300 nm as a function of the altitude in the atmosphere of Titan. According to their work, photons with wavelengths shorter than 150 nm do not penetrate below ~200 km, while photons in the 150 to 200 nm range are progressively absorbed from ~200 km to

~100 km. Finally, only photons in the 200–300 nm range penetrate below 100 km, down to ~50 km. Our recent experimental studies have demonstrated that these longer-wavelength (200 nm and above) ultraviolet (UV) photons could efficiently drive the photochemistry of ices, resulting in the production of organic polymers (Couturier-Tamburelli et al. 2014, 2015; Gudipati et al. 2013; Mouzay et al. 2021a,b) and to the photochemically driven incorporation of these molecules into existing haze particles (Couturier-Tamburelli et al. 2018; Fleury et al. 2019).

Our previous studies of pure-ice photochemistry in Titan's atmosphere were focused on acetylene (C_2H_2), benzene (C_6H_6), and some nitriles (hydrogen cyanide HCN, cyanoacetylene HC_3N , dicyanoacetylene C_4N_2 , and cyanodiacetylene HC_5N), as these species represent the composition of most identified ice clouds (Anderson & Samuelson 2011; Anderson et al. 2010, 2018b; de Kok et al. 2014; Khanna et al. 1987; Samuelson et al. 1997). However, higher hydrocarbons may also condense in Titan's stratosphere, as highlighted by the recent identification of ice clouds that contain benzene at Titan's south pole (Vinatier et al. 2018) and by the discovery by the Cassini Composite InfraRed Spectrometer (CIRS) of the High Altitude South Polar (HASP) cloud (Anderson et al. 2018b) whose spectral signature is consistent with co-condensed HCN- C_6H_6 ices

(Anderson et al. 2018b). After C_6H_6 , which we studied previously (Mouzay et al. 2021a,b), diacetylene (C_4H_2) is the next hydrocarbon to condense in the stratosphere of Titan at altitudes ranging from 70 to 130 km as a function of the latitude and the season according to different studies (Anderson et al. 2018b, 2016; Barth 2017). Intrigued by the lack of detection of condensed C_4H_2 either in the atmosphere or at the surface of Titan, we decided to focus our study on the photochemistry of C_4H_2 ice as a potential sink for condensed C_4H_2 in these environments.

In Titan's atmosphere, C_4H_2 is formed in the gas phase below 1200 km by the reaction of acetylene with C_2H radicals (Chastaing et al. 1998; Kaiser et al. 2002), while another mechanism involving the reaction of C_4H_3 with CH_3 radicals exists at higher altitude (Vuitton et al. 2019). Its mixing ratio varies significantly with altitude, decreasing from $\sim 7 \times 10^{-6}$ at 981 km in the ionosphere (Cui et al. 2009) to 1×10^{-9} in the stratosphere (Coustenis et al. 2007, 2010; Vinatier et al. 2007, 2010). In addition, the atmospheric mixing ratio of diacetylene is subject to seasonal variations, leading to a strong polar enrichment in the winter hemisphere (Coustenis et al. 2016; Sylvestre et al. 2018). Further, among the major unsaturated hydrocarbons, C_4H_2 has one of the most extended UV absorptions toward long wavelengths involving the $S_0 \rightarrow S_1$ (286 nm) and $S_0 \rightarrow T_1$ (387 nm) excitations (Fischer & Ross 2003; Vila et al. 2000) in addition to its strong photoabsorption cross section between 120 and 220 nm (Ferradaz et al. 2009). Our previous works have shown that direct photoexcitation from the singlet ground state to a triplet excited state is possible in the condensed phase (Couturier-Tamburelli et al. 2014; Gudipati et al. 2013). Therefore, diacetylene is an excellent candidate for solid-state photochemistry and a possible source for the formation of larger volatile molecules or organic polymers in the atmosphere of Titan. In addition, such a reactive photochemical sink could also potentially explain the lack of C_4H_2 -ice detection, whereas other ices such as HC_3N have been detected in Titan's atmosphere (Anderson et al. 2010, 2016). C_4H_2 is known to be photochemically reactive in the gas phase (Bandy et al. 1992, 1993; Delpech et al. 1994; Frost et al. 1995; Glicker & Okabe 1987), producing long carbon-chain species such as tri-acetylene (C_6H_2) and tetra-acetylene (C_8H_2). Therefore, C_4H_2 is suspected to be an important intermediate in the reaction pathways for the formation of large organic molecules that make up Titan's atmospheric haze (Abplanalp et al. 2019; Kaiser & Mebel 2012; Wilson & Atreya 2004). Another possibility is that the nondetection of C_4H_2 ice in Titan's atmosphere could be due to the existence of C_4H_2 co-condensate with another species such as HCN, that results in a modification of its spectral signature, as has been observed for the HC_3N -HCN or C_4N_2 -HCN co-condensate (Anderson et al. 2018a).

The work reported here presents the first experimental study of the photochemistry of diacetylene ice irradiated with near-UV ($\lambda > 300$ nm) photons. We studied the role of longer-wavelength UV-irradiation in the chemical evolution of C_4H_2 ices, the formation of volatile species, and organic polymers in the lower atmosphere of Titan. Finally, we assess the influence of the UV source (monochromatic vs. broadband) on the simulated photochemistry.

2. Experimental methods and analysis protocols

2.1. The TOAST and RING experimental setups

For this study we used the Titan Organic Aerosol SpecTroscopy (TOAST) experimental setup at the Jet Propulsion Laboratory, USA (Fleury et al. 2019; Gudipati et al. 2013), and the RING

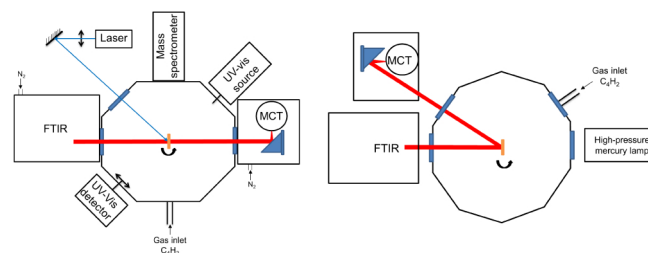


Fig. 1. Schemes of the TOAST experimental setup at JPL (left) and the RING experimental setup at PIIM (right).

experimental setup at the PIIM Laboratory at Aix-Marseille University, France (Theule et al. 2011). Figure 1 presents the schemes of the TOAST and RING setups. We decided to use these two experimental setups to obtain complementary datasets. As described in greater detail below, the two setups used infrared (IR) spectroscopy in transmission and reflection modes as well as complementary wavelength ranges. In addition, the experimental setup used at JPL used a monochromatic wavelength for the ice irradiation, while the setup at PIIM used a polychromatic UV source, which allowed us to study the possible differences in the chemistry between monochromatic and polychromatic irradiation.

Diacetylene is not available commercially and needs to be synthesized. For this study diacetylene was synthesized according to the method described in the literature (Khelifi et al. 1995), by the dropwise addition of 1,4-dichloro-2-butyne ($C_4H_4Cl_2$) to a mixture of potassium hydroxide (KOH), dimethyl sulfoxide (DMSO), and water maintained at a temperature of 72 °C under nitrogen flow atmosphere. DMSO serves to increase the solubility of C_4H_2 in the aqueous phase. At the end of the addition the temperature was increased to 95 °C and held at this temperature for 15 min. C_4H_2 gas was then driven off by bubbling N_2 gas through the liquid, passed through a calcium chloride ($CaCl_2$) trap to remove traces of water, and condensed in a trap cooled with liquid nitrogen (LN_2). Finally, C_4H_2 was purified by vacuum distillation and its purity was checked using mass spectrometry.

At JPL, ice films were formed by vapor deposition on a sapphire window fixed on the sample holder of a closed-cycle helium cryostat, located within a high vacuum chamber with a background pressure $\sim 8 \times 10^{-9}$ mbar. The cryostat has a resistive heater and a temperature controller to precisely control the temperature of the sample from 10 to 300 K. The temperature of the sample holder was measured using a silicon diode. In this study, C_4H_2 vapor was deposited from a gas line at a pressure of 1×10^{-6} mbar for 15 min on a sapphire window cooled to 70 K. This is lower than the temperature at which C_4H_2 could condense in Titan's atmosphere which is ~ 110 K for an altitude of ~ 70 km (Barth 2017; Lavvas et al. 2011). However, we made this choice based on different experimental constraints. First, a previous experimental study determined that diacetylene starts to sublime at ~ 100 K (Zhou et al. 2009) under a background pressure of $\sim 5 \times 10^{-9}$ mbar, similar to the pressures reached in our experimental chamber (i.e., $\sim 8 \times 10^{-9}$ mbar). It was therefore necessary to use a temperature lower than 100 K. We decided to use 70 K, a temperature much lower than 100 K, to avoid a possible slow sublimation of C_4H_2 during the irradiation experiments, which typically took several hours to complete. Sublimation could happen at any temperature in a high vacuum chamber because an ice is in equilibrium with its vapor phase. As the experimental chambers have turbopumps, vapor can be

pumped, inducing more and more sublimation of the ice over time. Nevertheless, the lower the temperature away from the sublimation temperature (~ 100 K), the weaker the ice's sublimation, and it was negligible at 70 K for the duration of the trial (which we experimentally determined).

The prepared ice film, about a micrometer thick (see Sect. 3.1), was subsequently irradiated for 6 h at 1 h doses, with photons at 355 nm obtained by a third harmonic generation from a nanosecond pulsed Nd:YAG laser (Quantel) with a repetition rate of 20 Hz. After each hour of irradiation, the spectra were measured before continuing the photolysis. The diameter of the initial circular laser beam was expanded from 3 to 20 mm using a plano-convex lens (75 mm focal length) that reduced the laser photons flux by a factor of 44 to uniformly illuminate the entire surface of the ice film and to avoid multi-photon processes. In a previous publication we showed that photons at 355 nm produced by a defocused nanosecond pulsed laser drove solid-phase photochemistry via a single-photon process (Gudipati et al. 2013), and one-photon absorption was shown to dominate even at 8 mJ pulse^{-1} or $9.1 \times 10^{16} \text{ photons cm}^{-2} \text{ s}^{-1}$ at 355 nm and 20 Hz repetition rate. The present work was carried out under similar conditions: at the same wavelength at 20 Hz repetition rate with an energy of $10.5 \text{ mJ pulse}^{-1}$ or $1.3 \times 10^{17} \text{ photons cm}^{-2} \text{ s}^{-1}$. Pulse energies were measured at the laser outlet, while photons fluxes were calculated at the sample's surface after expansion of the laser. The evolution of the diacetylene ice film was monitored after each irradiation using transmission-absorption IR and ultraviolet-visible (UV-Vis) spectroscopy. After irradiation, the sample was warmed to 180 K under vacuum using temperature-programmed desorption (TPD) at 1 K min^{-1} in order to sublimate the photo-produced volatiles. During the experiment, the composition of the sublimated gas-phase molecules was also monitored using in situ mass spectrometry.

At PIIM, ice films were formed by vapor deposition on a copper substrate fixed on the sample holder of a closed-cycle helium cryostat, located within a high vacuum chamber with a background pressure of $\sim 8 \times 10^{-9}$ mbar. The cryostat has a resistive heater and a temperature controller to precisely control the temperature of the sample from 10 K to 300 K. The temperature of the sample holder was measured using a silicon diode. We deposited 0.6 mbar of gas phase C_4H_2 for around 20 min on the copper surface kept at 70 K at a pressure of 1×10^{-6} mbar. In contrast to the JPL experiments where the ice was irradiated with a single wavelength laser, during the RING experiments, a diacetylene ice film (a few hundred nanometers thick; see Sect. 3.1) was irradiated with broadband UV photons ($\lambda > 300$ nm) generated by an Osram 200 W high-pressure mercury lamp equipped with a cutoff filter at 300 nm. The total photon flux of the lamp at wavelengths above 300 nm has been estimated to be about $2.75 \times 10^{16} \text{ photons cm}^{-2} \text{ s}^{-1}$ (Couturier-Tamburelli et al. 2014). After about 5 h of irradiation, the ice samples were slowly warmed up to room temperature to evaporate the volatile species. Changes in the ice samples were monitored by reflection IR spectroscopy.

2.2. IR spectroscopy

At JPL, IR spectra were recorded in transmission with a Thermo Scientific Nicolet 6700 Fourier Transform InfraRed (FTIR) spectrometer. After passing through the sample, the IR beam was focused on a mercury cadmium telluride (MCT) detector cooled to 77 K with LN_2 . Each spectrum consists of an average of 200 scans with a resolution of 1 cm^{-1} and covers the 1600 cm^{-1}

(sapphire cut on) to 4500 cm^{-1} range. Reflection absorption IR spectra were measured at PIIM from 4000 to 600 cm^{-1} using a Vertex 70 FTIR spectrometer. Each spectrum was averaged over 100 scans with a resolution of 1 cm^{-1} . At the copper surface the IR beam was reflected with a 36° angle and focused on a MCT detector cooled to 77 K. The two experiments at PIIM and JPL are therefore complementary in terms of spectral ranges, and provide a large spectral covering from 4500 to 600 cm^{-1} . The IR spectra recorded at JPL and PIIM were used to calculate the thickness of the deposited ice films and the diacetylene column density (see Sect. 3). To do this, we used the Beer-Lambert law. In the case of the reflection absorption spectra recorded at PIIM, this is an approximation that could bias the calculated values. Even so, this approach has been used in experimental studies using reflection absorption spectroscopy (Bennett & Kaiser 2005; Couturier-Tamburelli et al. 2018; Mouzay et al. 2021b; Noble et al. 2012). To take this problem into account and limit the error on the calculated values in the case of the PIIM experiments, we decided to divide the integrated absorbance in the equations used in Sect. 3 by a factor of 2 to correct for the incoming and outgoing infrared beam through the ice film.

2.3. UV-Vis spectroscopy

At JPL, the UV-Vis spectra were measured from 210 to 1100 nm with an incidence angle of 45° (Fig. 1), using an Ocean Optics DH-2000 deuterium-halogen lamp and a USB4000 spectrograph connected to the chamber via optical fiber feedthrough. Each spectrum was averaged over 500 scans with 20 ms of integration per scan.

2.4. Mass spectrometry

At JPL, the analysis by mass spectrometry of the molecules desorbed during the TPD was achieved with a quadrupole mass spectrometer (RGA 300, SRS instrument), with a mass range of 1–300 amu and equipped with a continuous dynode electron multiplier (CDEM) detector, enabling measurement of trace molecules at partial pressures as low as 1×10^{-12} mbar. The molecules were ionized by electron impact with an energy of 70 eV. The mass resolution ($m/\Delta m$) is 100 at m/z 100.

3. Results

3.1. Spectroscopy of C_4H_2 ice deposited at 70 K

Figure 2 presents the IR spectra of the diacetylene ice films deposited at 70 K at JPL and PIIM in the 3400 – 1800 cm^{-1} region and in the 4000 – 600 cm^{-1} region, respectively. Three fundamental absorption bands of C_4H_2 are observed in the JPL spectrum, in agreement with previous studies (Khanna et al. 1988; Zhou et al. 2009). The most intense peak at 3272 cm^{-1} is assigned to the ν_4 asymmetric stretching mode of the C–H bond. This band is saturated on the JPL spectrum because of the thick ice film used for the experiment (see discussion below). Weaker absorption bands at 2013 and 2177 cm^{-1} are assigned to the ν_5 asymmetric stretching mode and the ν_2 symmetric stretching mode of the $\text{C}\equiv\text{C}$ bond, respectively. Two other fundamental absorption bands of C_4H_2 are observed in the PIIM's spectrum located at 674 and 847 cm^{-1} and assigned to the ν_8 CH bending mode and to the ν_3 stretching mode of the C–C bond respectively. The position and shape of the absorption bands suggest that C_4H_2 is in a crystalline form when deposited at 70 K. This agrees with the previous experimental study of Zhou et al. (2009), which found

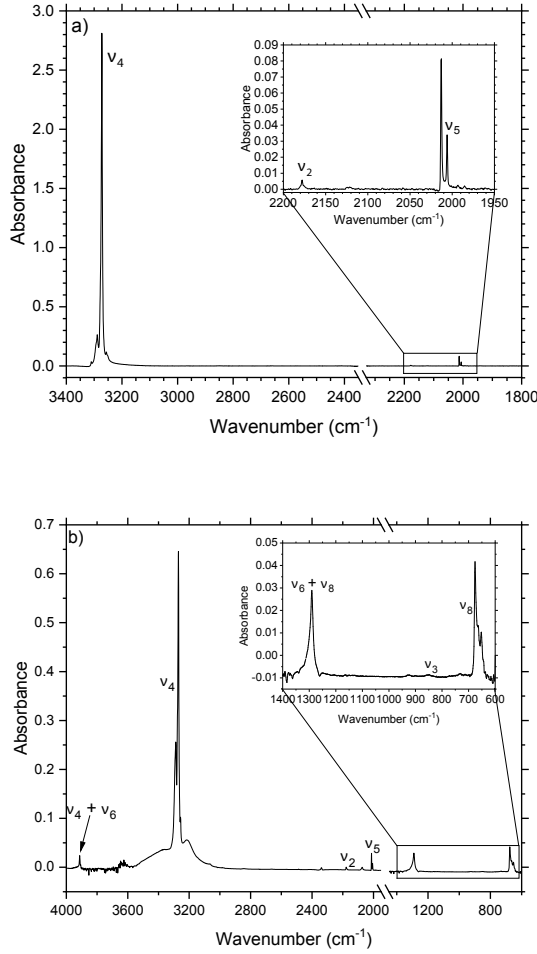


Fig. 2. Infrared spectra of C_4H_2 films obtained at JPL and PIIM independently. (a) IR spectrum of C_4H_2 ice deposited at 70 K at JPL on a sapphire window. The splitting of the ν_5 band is due to the crystalline nature of the ice film. The spectrum is cropped at 2340 cm^{-1} to remove the absorption band due to gas-phase CO_2 in the path of the IR beam outside the vacuum chamber. (b) IR spectrum of C_4H_2 ice deposited at 70 K at PIIM on a copper substrate.

that for C_4H_2 ice the amorphous to crystalline transition occurs around 70 K.

The diacetylene ice thickness h can be calculated as

$$h = \frac{\int \tau_\nu d\nu}{\int \alpha d\nu}, \quad (1)$$

where $\int \tau_\nu d\nu$ is the integrated optical depth of the band, which was determined from the absorbance of the band, and $\int \alpha d\nu$ is the integrated extinction coefficient of the band (cm^{-1}). For our calculation, we used an integrated extinction coefficient value of $3.9 \times 10^3\text{ cm}^{-1}$ for the 2013 cm^{-1} band, determined for crystalline diacetylene at 70 K by [Khanna et al. \(1988\)](#). We calculated a diacetylene ice thickness of $\sim 374\text{ nm}$ for the PIIM experiment and $\sim 1.1\text{ }\mu\text{m}$ for the JPL experiment, reflecting the difference in the deposition conditions between experiments carried out at JPL and PIIM. Although the thicker deposit used at JPL leads to a saturation of the C–H absorption band of C_4H_2 (see Fig. 2), we decided to proceed with this ice thickness to enhance the formation of volatile species and increase their detectability by IR and UV spectroscopy and mass spectrometry.

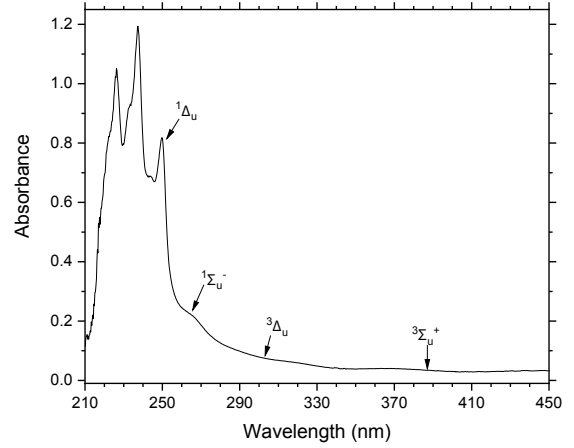


Fig. 3. UV spectrum of C_4H_2 ice deposited at 70 K at JPL on a sapphire window. The positions of the center of some electronic transitions of C_4H_2 are indicated (see discussion in Sect. 4.1).

As presented in Fig. 3, C_4H_2 ice at 70 K has strong absorption in the UV, with structured absorption bands at 226, 237, and 249 nm. These bands are separated by 2040 cm^{-1} wavenumbers, corresponding to ν_5 vibronic coupling in the singlet excited state $^1\Delta_u$. These absorption bands are close to those measured in the gas phase for C_4H_2 , but as expected they are shifted by $\sim 5\text{ nm}$ toward longer wavelengths compared to the gas-phase bands ([Jolly & Benilan 2008](#); [Smith et al. 1998](#)). However, in contrast to the gas phase, we observed in the solid phase the presence of a weaker absorption continuum from 250 to 400 nm.

3.2. Photochemistry of pure C_4H_2 ice at $\lambda > 300\text{ nm}$

At JPL the C_4H_2 ice film was irradiated for 6 hr with a 355 nm defocused laser. We monitored the gas-phase volatiles in the chamber using mass spectrometry during the irradiation and did not observe any photodesorption of diacetylene. In addition, IR and UV-Vis spectra were recorded after each irradiation period. We used the evolution of the diacetylene absorption bands at 3272 and 2013 cm^{-1} after each irradiation period to monitor its consumption due to photochemical reactions. Figure 4 (panels a and c) presents the evolution of the differential absorbance of these two absorption bands of C_4H_2 after each irradiation period. The differential absorbance is the difference between the absorbance after a time “ t ” of irradiation A_t and the initial absorbance $A_{t=0}$. After 1 h of irradiation we observed a small change in the C–H absorption band at 3272 cm^{-1} . However, this change is not conclusive (increase and decrease of the band) because of the saturation of the C–H absorption band at the beginning of the experiment (absorbance value $\gg 2.5$, Fig. 2). In addition, we observed a very small depletion of the ν_5 band at 2013 cm^{-1} . However, when we pursued the irradiation further, the absorbance of both diacetylene bands decreased, indicating a significant depletion of the ice sample. We also observed an increase in the absorbance at higher wavenumber, with broad peaks at 3284 and 3291 cm^{-1} as well as a larger continuum at higher wavenumber. This indicates the formation of new products from the C_4H_2 ice photochemistry. The peak at 3284 cm^{-1} may be attributed to vinylacetylene, C_4H_4 ([Kim & Kaiser 2009](#)). The same peak was observed in previous laboratory experiments involving acetylene ice photochemistry ([Cuyllé et al. 2014](#)).

The C_4H_2 ice film irradiation was performed at PIIM with a lamp generating photons at $\lambda > 300\text{ nm}$ in order to see

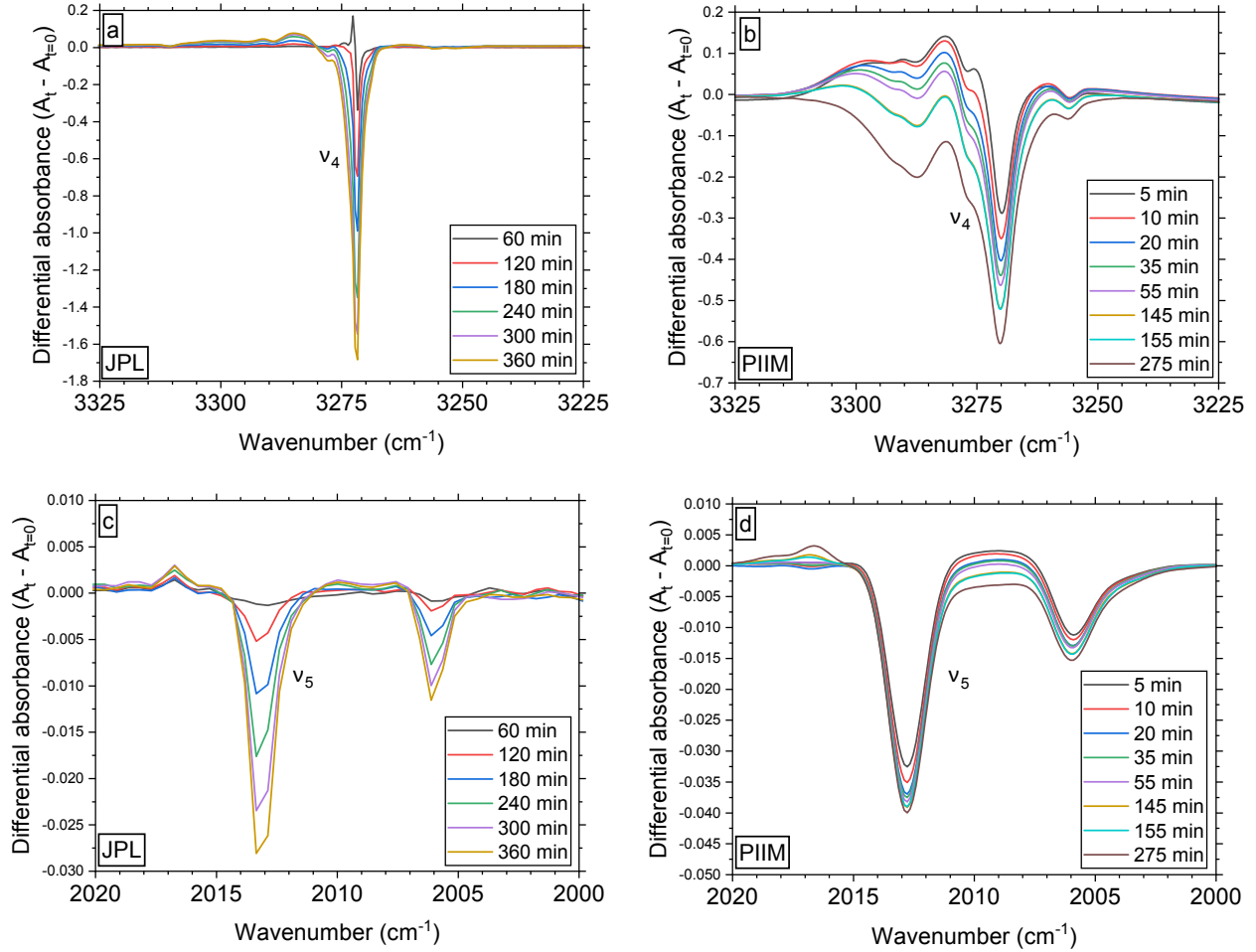


Fig. 4. Changes to IR spectra observed during near-UV irradiation of C_4H_2 ice films. (a) Evolution of the differential absorbance ($A_t - A_{t=0}$) of the ν_4 band of C_4H_2 as function of the time of irradiation at 355 nm at JPL. (b) Evolution of the differential absorbance of the ν_4 band of C_4H_2 as function of the time of irradiation at $\lambda > 300$ nm at PIIM. (c) Evolution of the differential absorbance of the ν_5 band of C_4H_2 as function of the time of irradiation at 355 nm at JPL. (d) Evolution of the differential absorbance of the ν_5 band of C_4H_2 as function of the time of irradiation at $\lambda > 300$ nm at PIIM.

if broadband irradiation leads to different results. Nevertheless, the results of these experiments are similar to those performed at JPL, as illustrated by the IR spectra shown in Fig. 4 (Panels b and d). The subtraction spectra reveal the appearance of new infrared bands, listed in Table 1, in addition to those observed at 3284 and 3291 cm^{-1} in the laser experiment. They are attributed without ambiguity to C_4H_4 when compared to the data of Kim & Kaiser (2009). From these results obtained at JPL and PIIM, we confirm that C_4H_4 is one of the photoproducts of C_4H_2 ice photochemistry. We note that the sapphire window used for transmission-absorption spectroscopy in the JPL experiments cuts off below 1600 cm^{-1} . For this reason, and based on the relative intensities of infrared bands obtained at PIIM, we observed only the ν_1 band of C_4H_4 in the JPL experiments. On the other hand, the PIIM experimental setup records the entire mid-infrared region thanks to the use of a reflection-absorption configuration. As a result, several absorption bands assigned to C_4H_4 are also observed in the experiments conducted at PIIM, increasing the confidence of our assignment. We also note that in the transmission-absorption mode employed at JPL, the sample is ~ 1100 nm thick, which is also the IR beam pathlength. Under reflection-absorption conditions, the IR beam penetrates through longer than twice the ice thickness of 374 nm. For this reason, we could be sampling twice the amount of the ice.

We derived the evolution of the C_4H_2 column density consumed as a function of the photon fluences for both experiments from the IR data shown in Fig. 4. We decided to calculate the column density using the integrated ν_5 band area of C_4H_2 at 1203 cm^{-1} because the other band at 3272 cm^{-1} was saturated. The consumed column density can be calculated with Eq. (2),

$$N_c = N_0 - N_f, \quad (2)$$

where N_c is the consumed column density (molecules cm^{-2}) after a fluence f , N_0 is the initial column density (molecules cm^{-2}) of C_4H_2 , and N_f is the column density (molecules cm^{-2}) of C_4H_2 molecules remaining after a fluence f . The column density is determined using Eq. (3),

$$N = \frac{\int \tau_\nu d\nu}{A}, \quad (3)$$

where N is the column density (molecules cm^{-2}), A is the band strength (cm molecule $^{-1}$), and $\int \tau_\nu d\nu$ is the integrated band in optical depth derived from the absorbance. The band strength A can be calculated from the integrated extinction coefficient using Eq. (4),

$$A = \frac{\int \alpha d\nu}{\rho_N}, \quad (4)$$

Table 1. Infrared absorption bands of C₄H₄ ice observed in our experimental conditions.

Assignment	Kim & Kaiser (2009) 100 K Position (cm ⁻¹)	JPL 70 K Position (cm ⁻¹)	PIIM 70 K Position (cm ⁻¹)	PIIM 70 K Relative intensity
ν_1	3288	3291/3284	3290/3281	100
ν_3	3049		3037	1.5
ν_4	3014		3017	2.1
$\nu_6 + \nu_7$			2965	0.5
ν_5	2103		2104	2.0
ν_6	1599		1592	0.9
$\nu_{10} + \nu_{12}$	1374		1384	10.3
$2\nu_{11}/2\nu_{17}/\nu_{11} + \nu_{17}$	1259		1262	15.9

Notes. The position of the absorption bands observed after irradiation in the JPL and PIIM experiments at 70 K is shown. The position of the IR absorption bands of crystalline C₄H₄ ice at 100 K determined experimentally by Kim & Kaiser (2009) is also shown for reference. Relative intensities of the IR bands observed in the PIIM experiment were calculated from the integrated areas of the IR bands.

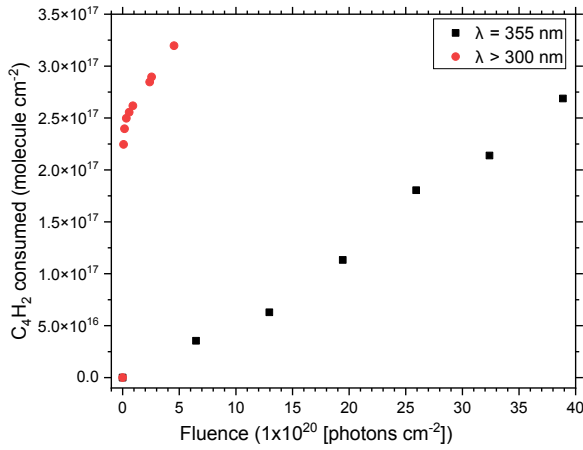


Fig. 5. Quantity of C₄H₂ consumed as a function of the photon-fluence (JPL, 355 nm, black square; PIIM, $\lambda > 300$ nm, red circle). The quantity is expressed in column density and was calculated from the IR spectra.

where $\int \alpha dv$ is the integrated extinction coefficient (cm⁻¹) and ρ_N is the number density (molecules cm⁻³). Finally, by combining Eqs. (3) and (4), we obtained Eq. (5):

$$N = \frac{\int \tau_\nu dv \times \rho_N}{\int \alpha dv}. \quad (5)$$

For our calculation we used an integrated extinction coefficient value of 3.9×10^3 cm⁻² for the 2013 cm⁻¹ band calculated for the crystalline diacetylene at 70 K by Khanna et al. (1988) and a ρ_N of 9.2×10^{21} molecules cm⁻³. The value of the number density is the more important source of uncertainties for this calculation and this value is derived from the mass density using Avogadro's number, and the molar mass of diacetylene (50.06 g mol⁻¹). However, the mass density of crystalline diacetylene is not available in the literature. Thus, we assumed a mass density of 0.76 g cm⁻³ measured for crystalline acetylene at 131 K (Hudson et al. 2014; McMullan et al. 1992). Figure 5 presents the evolution of the consumed C₄H₂ in column density as a function of the photon-fluence for both experiments performed at JPL and PIIM. As explained in Sect. 2.2, a doubled pathlength of absorption due to the reflection-absorption technique used at PIIM was factored in when calculating the column density for the PIIM experiments. We obtained that 2.6×10^{17} molecule cm⁻² of C₄H₂ were

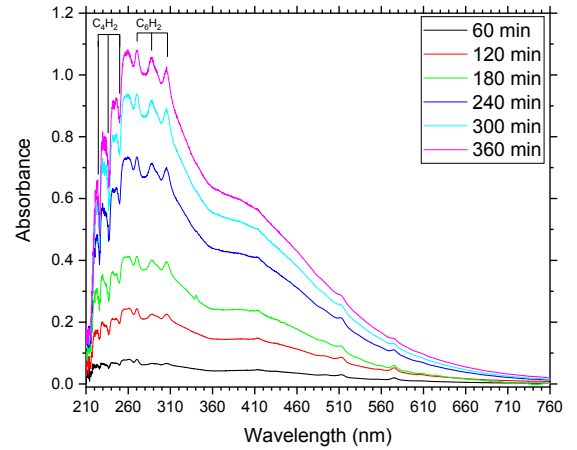


Fig. 6. Differential absorbance ($A_t - A_{t=0}$) in the UV-Vis domain for the different time of irradiation at 355 nm. Assignments of some of the absorption bands are shown.

consumed for a photon-fluence of 3.9×10^{21} photons cm⁻² at 355 nm, while 3.4×10^{17} molecule cm⁻² of C₄H₂ were consumed for a fluence of 4.5×10^{20} photons cm⁻² at $\lambda > 300$ nm. These results indicate that a polychromatic photon flux covering a broader wavelength range longward of 300 nm substantially increases the kinetics of the diacetylene photolysis, leading to a slightly higher number of diacetylene molecules consumed with a photon fluence that is ten times lower compared to irradiation performed at 355 nm. We can make the hypothesis that this difference is due to a significant increase in the absorbance of diacetylene between 350 and 300 nm (Fig. 3).

The UV-Vis spectra obtained during the experiments at JPL are presented in Fig. 6; they provide complementary information on the photochemistry of C₄H₂ upon irradiation at 355 nm. We observed the diminution of the diacetylene absorption bands after 60 min of irradiation and then after each successive step of irradiation, in agreement with the IR measurements. In addition, new absorption bands were observed at longer wavelengths: 270, 287, 306, 414, 513, and 575 nm. In addition to these individual bands, we observed an increase in continuum from 260 to 700 nm after each irradiation. A similar absorption continuum was also observed during previous experiments on C₄N₂ ice (Gudipati et al. 2013) and can be attributed to the growth of a polymeric organic material in the ice. The new bands can

be attributed to the production of new species. The bands at 270, 287, and 306 nm can be tentatively assigned to C_6H_2 . In the gas phase C_6H_2 has strong absorption bands located at 260, 275, and 293 nm (Jolly & Benilan 2008; Shindo et al. 2003). In the solid phase we observed a shift of the absorption bands of C_6H_2 toward longer wavelengths by about 10 nm compared to the gas phase, as also observed for C_4H_2 . We did not observe absorption bands of C_6H_2 in the infrared, but the C_6H_2 absorption bands are most likely buried under the C_4H_2 bands (particularly in the C-H stretch region), which prevents its identification by IR spectroscopy. Other absorption bands at longer wavelengths could not be attributed to a specific compound. Nevertheless, polycyclic aromatic compounds (PAHs) are good candidates to explain these absorption bands because the formation of PAHs has been observed in another experimental study after the irradiation of acetylene ice (C_2H_2) with low-energy electrons (Abplanalp et al. 2019). Further, several PAHs, such as phenanthrene ($C_{14}H_{10}$), perylene ($C_{20}H_{12}$; Salama et al. 2011), or larger PAHs (Ruiterkamp et al. 2002), have a strong absorption in the UV at wavelengths shorter than 300 nm and additional weaker absorption bands at longer wavelengths, similar to those observed in Fig. 6. However, the fundamental transition of these PAHs overlaps with the absorption bands of other volatiles, such as C_6H_2 , and with the absorption continuum of the polymer. The UV-Vis spectra alone are not specific enough to identify, if formed during the experiments, a single PAH among many other photoproducts. Future work employing other analytical techniques such as chromatography mass spectrometry could provide a better identification of these molecules.

3.3. Temperature-programmed desorption (TPD) of the ice after irradiation

After the irradiation of the diacetylene ice at JPL, the sample was warmed under vacuum from 70 to 180 K with a ramp of 1 K min^{-1} to sublimate all the volatile species formed during irradiation (180 K is the lowest temperature to observe the sublimation of all volatiles). Desorption of several species was tracked as a function of the sample temperature using in situ mass spectrometry. After preliminary experiments in which we recorded mass spectra from m/z 1 to 200 during TPD experiments, we decided to track the thermal desorption of C_4H_2 ($C_4H_2^+$, m/z 50) and its hydrogenation products detected by IR spectroscopy, C_4H_4 ($C_4H_4^+$, m/z 52). We also monitored the thermal desorption of other, more saturated C4 species: butyne C_4H_6 ($C_4H_6^+$, m/z 54), butene C_4H_8 ($C_4H_8^+$, m/z 56), and butane (C_4H_{10}) using its major fragmentation peak ($C_3H_7^+$, m/z 43) as the proxy. Finally, we tracked the thermal desorption of C_6H_2 ($C_6H_2^+$, m/z 74), which was identified using UV-Vis spectroscopy. We did not observe an increase in the intensity at other masses, except for those corresponding to fragments of these molecules. Figure 7 presents the temperature-dependent desorption profile for m/z 43, 50, 52, 54, 56, and 74.

The C_4H_2 ice remaining after the irradiation is the most abundant species detected during the TPD. Its desorption started at ~ 80 K with a first peak at 90 K, while the maximum of desorption occurred at ~ 120 K; a last peak is visible at ~ 150 K. In a previous study crystalline C_4H_2 was found to start desorbing at ~ 100 K with maxima at 120 and ~ 150 K (Zhou et al. 2009). Therefore, our results agree with this previous study. The ion signal at m/z 52 starts to increase at 100 K with a maximum at 120 K, and can be attributed to the desorption of C_4H_4 , which was also detected using IR spectroscopy. Finally, ion signals at m/z 43, 54, 56, and 74 started to increase at 110 K with maxima

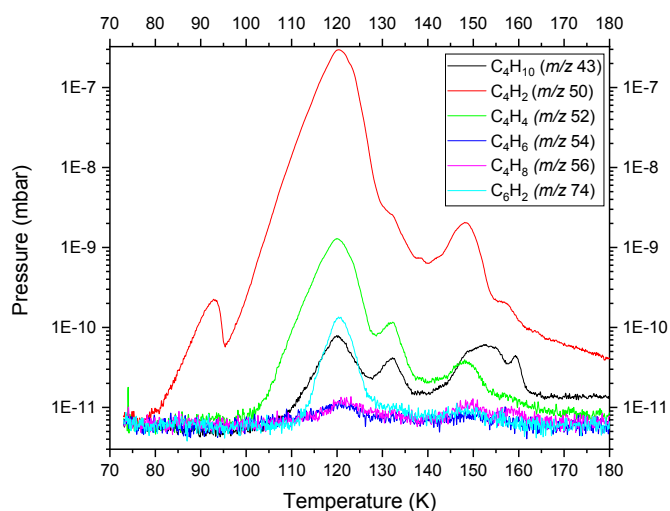


Fig. 7. Temperature desorption profile of m/z 43 ($C_3H_7^+$, main fragment of C_4H_{10}), 50 ($C_4H_2^+$), 52 ($C_4H_4^+$), 54 ($C_4H_6^+$), 56 ($C_4H_8^+$), and 74 ($C_6H_2^+$) after irradiation of C_4H_2 with a laser at 355 nm. The sample was heated (1 K min^{-1}) from 70 to 180 K.

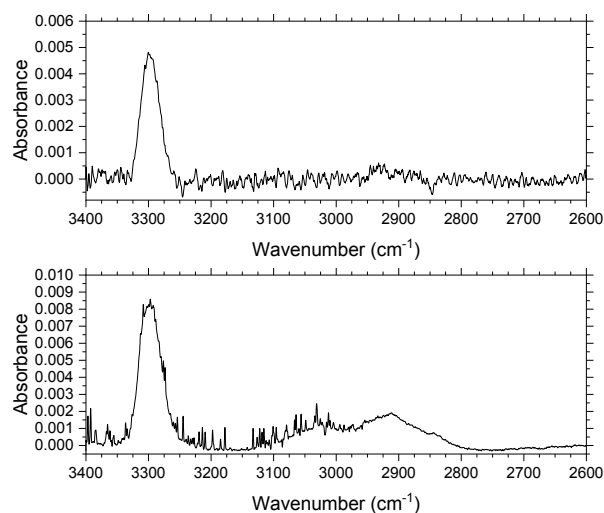


Fig. 8. Infrared spectra obtained from non-volatile residue subsequent to C_4H_2 photolysis. Top: IR absorption spectrum of the organic polymer produced during the JPL experiment. Bottom: IR absorption spectrum of the organic polymer produced during the PIIM experiment. The spectra were recorded at ambient temperature at the end of the experiments.

at 120 K, coinciding with maximum desorption of C_4H_2 . C_4H_4 is the main volatile product of the C_4H_2 photochemistry detected during the TPD followed by C_6H_2 and C_4H_{10} (based on $C_3H_7^+$, the C_4H_{10} main fragment). Ion signal variations at m/z 54 and 56 were very low, showing that these two species were produced in a negligible amount compared to the three other hydrocarbons produced. It is likely that C_4H_6 and C_4H_8 are highly reactive compared to the other products.

3.4. Organic residues spectra

At the end of the TPD run, each sample was further warmed to room temperature. Figure 8 presents the IR spectra of the organic residues remaining, on the sapphire window (top) in the JPL studies and on the copper surface (bottom) in the PIIM studies, after the sublimation of the ices at room temperature under vacuum. These residues are lightly colored (brownish).

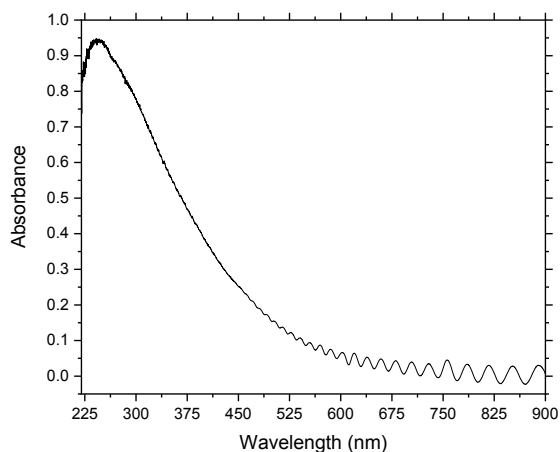


Fig. 9. UV-Vis absorption spectrum of the organic polymer produced during the JPL experiment. The spectrum was recorded at ambient temperature at the end of the experiment.

Both IR spectra (JPL and PIIM) show an intense absorption band $\sim 3300\text{ cm}^{-1}$, as illustrated in Fig. 8, attributed to stretching $\equiv\text{CH}$. The position and shape of this absorption band of the polymer are similar for the two different C_4H_2 ice photochemistry studies (355 nm laser irradiation at JPL and $\lambda > 300\text{ nm}$ Hg lamp irradiation at PIIM). However, the spectra of the organic films generated at JPL and at PIIM (Fig. 8) also show significant differences between 3100 and 2800 cm^{-1} . The lower-frequency absorptions between 3100 and 3000 cm^{-1} (due to alkene and aromatic C–H stretch) seen in the PIIM studies are consistently absent in the JPL studies, indicating that the broad range of wavelengths used in the PIIM irradiation (unlike the single laser wavelength used during the JPL experiments) resulted in more unsaturated and aromatic hydrocarbons.

In addition to the IR spectroscopy, the absorption spectrum of the polymer was recorded in the UV-Vis for the sample produced at JPL. The spectrum is presented in Fig. 9. At room temperature, the organic residue presents an intense absorption continuum in the UV, which decreases exponentially in the visible and extends up to 600 nm. Observations of interference fringes between 500 and 900 nm indicate that the polymer residue forms a nonscattering and homogeneous film on the sapphire window. The continuum absorption of the residue does not differ significantly from that observed at 70 K (Fig. 6), indicating that a large part of the polymer is formed during the irradiation of the ice. We observed at room temperature that all the absorption bands attributed previously to C_4H_2 , C_6H_2 , and tentatively to PAHs have disappeared, leaving only a large continuum. This indicates that most of these species are volatile at room temperature under vacuum, as illustrated by the detection of desorbed C_4 hydrocarbons and C_6H_2 by mass spectrometry during the TPD (Fig. 7). It is also likely that thermal reactions could occur between volatile compounds or between volatile compounds and the polymer during the warming up of the sample, modifying the composition of the polymer, which would be reflected in its UV-Vis absorption spectrum.

4. Discussions

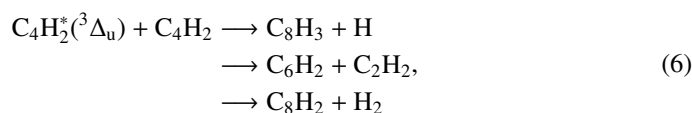
4.1. Chemical pathways for hydrocarbon formations

Our experiments point out that C_4H_2 is photochemically highly active in the solid phase, leading to the formation of C_6H_2 and

hydrogenated products (C_4H_4 , C_4H_6 , C_4H_8 , and C_4H_{10}). However, we did not find clear evidence of the formation of C_8H_2 , which was observed previously in the gas phase irradiation of C_4H_2 (Bandy et al. 1992, 1993). Although it is difficult to identify the reaction mechanism in our experimental conditions, based on literature data (Bandy et al. 1992, 1993), we can try to propose chemical pathways for the formation of the different species observed.

During the JPL experiments, irradiation of C_4H_2 with the laser at $\lambda = 355\text{ nm}$ (3.49 eV or $\sim 28\,169\text{ cm}^{-1}$) can provide enough energy to excite C_4H_2 into the second lowest excited state $^3\Delta_u$, extended between 3.2 and 4.7 eV ($\sim 263\text{ nm}$ or $\sim 38\,023\text{ cm}^{-1}$ and $\sim 400\text{ nm}$ or $\sim 25\,000\text{ cm}^{-1}$) in the gas phase, as predicted by Allan (1984) and Bandy et al. (1993). This also suggests that the JPL experiments could access the first triplet excited state $^3\Sigma_u^+$ centered at 3.2 eV ($\sim 387\text{ nm}$ or $\sim 25\,800\text{ cm}^{-1}$), which should be involved in the photochemistry observed. Hence, the observed photochemistry must be mediated by the two lowest triplet states ($^3\Sigma_u^+$ or $^3\Delta_u$) reached through direct excitation from the ground singlet state, similar to the mechanism proposed for the C_4N_2 ice photochemistry (Gudipati et al. 2013).

Likewise, for the experiments conducted at PIIM with $\lambda > 300\text{ nm}$ ($E < 4.13\text{ eV}$ or $\sim 33\,333\text{ cm}^{-1}$), we can access the UV absorption bands below 4.13 eV. As seen from Fig. 3, and as in the case of the JPL experiments, C_4H_2 can be also excited into the two first excited states $^3\Sigma_u^+$ or $^3\Delta_u$ (Allan 1984) with the lamp and filter combination used at PIIM. However, these two kinds of irradiation ($\lambda = 355\text{ nm}$ and $\lambda > 300\text{ nm}$) are not sufficient to excite the $^1\Sigma_u^-$ (4.8 eV or $\sim 38\,800\text{ cm}^{-1}$) or $^1\Delta_u$ (5.1 eV or $\sim 40\,800\text{ cm}^{-1}$), which are known to induce the $\text{C}_4\text{H} + \text{H}$ and C_2H formation (Bandy et al. 1993). According to the work of Bandy et al. (1993) and more recently Vuitton et al. (2019), at the wavelengths of our work at PIIM or JPL, photochemical reactions are supposed to be initiated from the metastable higher triplet excited state of C_4H_2 , instead of the direct photolysis. These reaction channels are illustrated below. They can explain the formation of three compounds observed during our irradiation experiments namely C_4H_4 , C_4H_6 , and C_6H_2 :



Bandy et al. (1993) proposed additional routes for the formation of secondary species via the reaction of C_4H_2 with primary products, as illustrated by reaction (9):



This secondary reaction could explain the nondetection of C_8H_2 at the end of our experiment. Bandy et al. (1993) explained that the C_6H_2 formation induces the production of C_2H_2 , as previously illustrated in reaction (6). In addition, work from Glicker & Okabe (1987) suggests that C_4H_2 photopolymerization occurred via molecular mechanisms, free radicals being detected only at $\lambda < 180\text{ nm}$, so it seems highly probable that in both our experiments at JPL and PIIM (irradiations performed at $\lambda > 300\text{ nm}$ and $\lambda = 355\text{ nm}$) the photochemistry occurred through the metastable triplet excited state pathway and not through the

involvement of singlet excited states. Similarly, the formation of C_4H_4 seems to be driven by the reaction of $C_4H_2^*$ and H in solid phase (Arrington et al. 1998), as depicted by (reaction (7)). Based on the above analysis, we conclude that C_4H_2 ice photochemistry is driven by the direct photoexcitation into the triplet excited states, as previously observed with C_4N_2 ice (Gudipati et al. 2013). At least, C_4H_8 and C_4H_{10} could be formed by successive addition of 2H on C_4H_6 and C_4H_8 . Such photochemistry is accessible only in the condensed phase, where the spin-selection rules are relaxed for the absorption of a photon by a molecule with other molecules, making ground-state singlet to excited state triplet transitions weakly allowed. As a result, longer-wavelength photons can be absorbed through these transitions and can initiate photochemical reactions.

4.2. Implications for Titan's atmospheric and surface chemistry

Our experimental results reveal that the exposure of diacetylene ice particles to near-UV photons ($\lambda > 300$ nm) could drive a complex organic chemistry in Titan's lower atmosphere. However, our results point out that the kinetics of the diacetylene photochemistry vary significantly as a function of the wavelength of the photons used for the irradiation. Our experiments at JPL show that a significant amount of photon fluence (3.9×10^{21} photons cm^{-2}) is necessary with a monochromatic laser irradiation at 355 nm to obtain a moderate depletion of diacetylene ice. However, with a polychromatic photon flux (which is expected on Titan) covering wavelengths down to 300 nm, the kinetic of the diacetylene photolysis drastically increases leading to similar diacetylene molecules consumption with a fluence (4.5×10^{20} photons cm^{-2}) ten times lower compared to the monochromatic experiments. We can qualitatively understand this difference as being due to a significant increase in the absorbance of diacetylene between 350 and 300 nm (Fig. 3) as well as broadband polychromatic lamp versus monochromatic laser as the photolysis source. Nevertheless, the flux of photons used in our experiments is orders of magnitude larger than that reaching the stratosphere and the troposphere of Titan. To enable a more rigorous quantification of our laboratory data in regard to Titan's conditions, it is necessary to have better modeling studies that estimate photon fluxes at different wavelengths below 350 nm and at different altitudes in Titan's atmosphere. This estimation would allow us to quantify the fraction of the diacetylene ice that could be photolyzed in the atmosphere of Titan during the ice particles sedimentation before reaching the surface.

Moreover, this would allow us to quantify the impact of the solid-phase photochemistry for the composition of Titan's lower atmosphere. This solid-phase chemistry could act as a sink for volatile species such as C_4H_2 in Titan's lower atmosphere and provide a source for other volatile hydrocarbons such as C_6H_2 , although these products may be trapped in the ice phase depending on the pressure and temperature. We also expect other atmospheric molecules to precipitate and accrete onto the ice at lower altitudes all the way to the surface. Other major atmospheric molecules of Titan such as HCN and other nitriles, which are known constituents of Titan's ice clouds (Anderson & Samuelson 2011; Anderson et al. 2010; de Kok et al. 2014; Samuelson et al. 1997), could undergo similar reactivity in the solid phase. An analysis of the spectral signatures of ice clouds suggests that those ice particles could be made of co-condensed molecular species (Anderson et al. 2018a). In the case of the co-condensation of a hydrocarbon such as C_4H_2 and a

nitrogen-bearing species such as HCN or HC_3N , solid-phase reactivity likely leads to a coupling of the nitrogen and hydrocarbon chemistry and may initiate the formation of nitrogen containing complex organics, including N-PAHs and possibly biologically important molecules such as adenine ($C_5H_5N_5$). Overall, this solid-phase reactivity plays an important role in determining the composition of the organic material formed in the atmosphere and that will ultimately contribute to the complex organic molecular, ice, and aerosol diversity on Titan's surface, whose composition will be studied by the future Dragonfly mission.

5. Conclusions

Titan's atmosphere is enriched with simple hydrocarbons and nitriles. Some of the most abundant molecules are detected both in the gas phase and in the condensed phase in the atmosphere. Diacetylene is one exception, which is detected in the gas phase but not in the condensed phase. Non-detection of C_4H_2 in the atmospheric ice clouds as well as on the surface of Titan has been a puzzle, for which the results of our laboratory experiments provide a potential rationale:

1. We studied experimentally the photochemistry of solid diacetylene at 70 K under irradiation with photons at wavelengths longer than 300 nm, closely simulating the radiations received by ice particles in Titan's atmosphere. Our experimental results have shown that diacetylene ice is very reactive under these conditions. A total of 2.6×10^{17} molecules cm^{-2} of C_4H_2 were consumed after a photon-fluence of 3.9×10^{21} photons cm^{-2} at 355 nm while 3.4×10^{17} molecules cm^{-2} of C_4H_2 were consumed after a photon-fluence of 4.5×10^{20} photons cm^{-2} at $\lambda > 300$ nm, indicating increasing photochemistry yields with decreasing photon wavelengths between 355 nm and 300 nm;
2. We analyzed the evolution of the composition of the solid phase after irradiation using IR and UV-Vis spectroscopy. In addition, we used TPD to analyze the composition of the desorbed species using in situ mass spectrometry. Our results show that the diacetylene photochemistry follows different pathways leading to the formation of different volatile species as well as an organic residue. First, we observed hydrogenation of C_4H_2 to form other C_4H_{2n} ($n = 2-5$) hydrocarbons. The main photoproduct was C_4H_4 and then C_4H_{10} , while C_4H_6 and C_4H_8 were produced in a negligible amount. Second, the photochemistry of C_4H_2 ice also resulted in the production of larger and highly polymerizable hydrocarbons such as C_6H_2 , and presumably aromatics compounds such as PAHs;
3. Finally, we observed the very efficient formation of a tholin-like organic polymer that is stable at room temperature, which has a strong absorption continuum at UV-Vis wavelengths, monotonically decreasing from 200 to 600 nm. Beyond 600 nm no absorption was detected, indicating that the photopolymer could be photochemically activated with photons at wavelengths between 250 and 600 nm either in Titan's troposphere and stratosphere or on the surface. These results agree with our earlier work on other tholins, indicating that this is the general behavior of Titan's organic aerosol analogs;
4. Although diacetylene ice has not been observed yet on Titan, our experimental results highlight the importance that this compound could have for the ice photochemistry in Titan's troposphere and stratosphere. A significant amount of C_4H_2

ice could be transformed into other volatile molecules, and into organic polymers, and so provide a significant loss process for diacetylene. It is likely that in the case of co-condensation of two or more volatiles, C₄H₂ could trigger the photochemistry through reaction with other hydrocarbons or nitriles, initiating a more complex chemistry in the solid phase.

Acknowledgements. Some of this work was carried out at the Jet Propulsion Laboratory, California Institute of Technology under a contract with the National Aeronautics and Space Administration. The JPL part of the work was supported by the NASA Solar System Workings and New Frontiers Data Analysis programs. The work carried out at the Physique des Interactions Ioniques et Moléculaires (PIIM) laboratory, Aix-Marseille Université, was supported by the Programme National de Planétologie (PNP).

References

- Abplanalp, M. J., Frigge, R., & Kaiser, R. I. 2019, *Sci. Adv.*, **5**, eaaw5841
- Allan, M. 1984, *J. Chem. Phys.*, **80**, 6020
- Anderson, C. M., & Samuelson, R. E. 2011, *Icarus*, **212**, 762
- Anderson, C. M., Samuelson, R. E., Bjoraker, G. L., & Achterberg, R. K. 2010, *Icarus*, **207**, 914
- Anderson, C. M., Samuelson, R. E., Yung, Y. L., & McLain, J. L. 2016, *Geophys. Res. Lett.*, **43**, 3088
- Anderson, C. M., Nna-Mvondo, D., Samuelson, R. E., McLain, J. L., & Dworkin, J. P. 2018a, *ApJ*, **865**, 62
- Anderson, C. M., Samuelson, R. E., & Nna-Mvondo, D. 2018b, *Space Sci. Rev.*, **214**
- Arrington, C. A., Ramos, C., Robinson, A. D., & Zwier, T. S. 1998, *J. Phys. Chem. A*, **102**, 3315
- Bandy, R. E., Lakshminarayan, C., Frost, R. K., & Zwier, T. S. 1992, *Science*, **258**, 1630
- Bandy, R. E., Lakshminarayan, C., Frost, R. K., & Zwier, T. S. 1993, *J. Chem. Phys.*, **98**, 5362
- Barth, E. 2003, *Icarus*, **162**, 94
- Barth, E. L. 2017, *Planet. Space Sci.*, **137**, 20
- Bennett, C. J., & Kaiser, R. I. 2005, *ApJ*, **635**, 1362
- Chastaing, D., L. James, P., R. Sims, I., & W. M. Smith, I. 1998, *Faraday Discuss.*, **109**, 165
- Coustenis, A., Achterberg, R. K., Conrath, B. J., et al. 2007, *Icarus*, **189**, 35
- Coustenis, A., Jennings, D. E., Nixon, C. A., et al. 2010, *Icarus*, **207**, 461
- Coustenis, A., Jennings, D. E., Achterberg, R. K., et al. 2016, *Icarus*, **270**, 409
- Couturier-Tamburelli, I., Gudipati, M. S., Lignell, A., Jacovi, R., & Piétri, N. 2014, *Icarus*, **234**, 81
- Couturier-Tamburelli, I., Piétri, N., & Gudipati, M. S. 2015, *A&A*, **578**, A111
- Couturier-Tamburelli, I., Piétri, N., Le Letty, V., Chiavassa, T., & Gudipati, M. 2018, *ApJ*, **852**, 117
- Cui, J., Yelle, R. V., Vuitton, V., et al. 2009, *Icarus*, **200**, 581
- Cuyille, S. H., Zhao, D., Strazzulla, G., & Linnartz, H. 2014, *A&A*, **570**, A83
- de Kok, R., Irwin, P. G. J., & Teanby, N. A. 2008, *Icarus*, **197**, 572
- de Kok, R. J., Teanby, N. A., Maltagliati, L., Irwin, P. G. J., & Vinatier, S. 2014, *Nature*, **514**, 65
- Delpech, C., Guillemin, J. C., Paillous, P., et al. 1994, *Spectrochim. Acta A Mol. Spectrosc.*, **50**, 1095
- Ferradaz, T., Bénilan, Y., Fray, N., et al. 2009, *Planet. Space Sci.*, **57**, 10
- Fischer, G., & Ross, I. G. 2003, *J. Phys. Chem. A*, **107**, 10631
- Fleury, B., Gudipati, M. S., Couturier-Tamburelli, I., & Carrasco, N. 2019, *Icarus*, **321**, 358
- Frost, R. K., Zavarin, G. S., & Zwier, T. S. 1995, *J. Phys. Chem.*, **99**, 9408
- Frère, C., Raulin, F., Israel, G., & Cabane, M. 1990, *Adv. Space Res.*, **10**, 159
- Fulchignoni, M., Ferri, F., Angrilli, F., et al. 2005, *Nature*, **438**, 785
- Glicker, S., & Okabe, H. 1987, *J. Phys. Chem.*, **91**, 437
- Gudipati, M. S., Jacovi, R., Couturier-Tamburelli, I., Lignell, A., & Allen, M. 2013, *Nat. Commun.*, **4**, 1648
- Hudson, R. L., Ferrante, R. F., & Moore, M. H. 2014, *Icarus*, **228**, 276
- Jolly, A., & Benilan, Y. 2008, *J. Quant. Spectrosc. Radiative Transfer*, **109**, 963
- Kaiser, R. I., & Mebel, A. M. 2012, *Chem. Soc. Rev.*, **41**, 5490
- Kaiser, R. I., Stahl, F., Schleyer, P. v. R., & Schaefer, H. F. III, 2002, *Phys. Chem. Chem. Phys.*, **4**, 2950
- Khanna, R. K., Perera-Jarmer, M. A., & Ospina, M. J. 1987, *Spectroch. Acta A Mol. Spectrosc.*, **43**, 421
- Khanna, R. K., Ospina, M. J., & Zhao, G. 1988, *Icarus*, **73**, 527
- Khelifi, M., Paillous, P., Delpech, C., et al. 1995, *J. Mol. Spectrosc.*, **174**, 116
- Kim, Y. S., & Kaiser, R. I. 2009, *ApJS*, **181**, 543
- Lavvas, P., Griffith, C. A., & Yelle, R. V. 2011, *Icarus*, **215**, 732
- Lavvas, P., Yelle, R. V., Koskinen, T., et al. 2013, *PNAS*, **110**, 2729
- Liang, M.-C., Yung, Y. L., & Shemansky, D. E. 2007, *ApJ*, **661**, L199
- Mayo, L. A., & Samuelson, R. E. 2005, *Icarus*, **176**, 316
- McMullan, R. K., Kvik, A., & Popelier, P. 1992, *Acta Crystallogr. B*, **48**, 726
- Mouzay, J., Couturier-Tamburelli, I., Piétri, N., & Chiavassa, T. 2021a, *J. Geophys. Res. Planets*, **126**, e2020JE006566
- Mouzay, J., Henry, K., Ruf, A., et al. 2021b, *Planet. Sci. J.*, **2**, 37
- Noble, J. A., Theule, P., Mispelaer, F., et al. 2012, *A&A*, **543**, A5
- Raulin, F., & Owen, T. 2002, *Space Sci. Rev.*, **104**, 377
- Ruiterkamp, R., Halasinski, T., Salama, F., et al. 2002, *A&A*, **390**, 1153
- Sagan, C., & Reid Thompson, W. 1984, *Icarus*, **59**, 133
- Salama, F., Galazutdinov, G. A., Krelowski, J., et al. 2011, *ApJ*, **728**, 154
- Samuelson, R. E., & Mayo, L. A. 1991, *Icarus*, **91**, 207
- Samuelson, R. E., Mayo, L. A., Knuckles, M. A., & Khanna, R. J. 1997, *Planet. Space Sci.*, **45**, 941
- Shindo, F., Benilan, Y., Guillemin, J. C., et al. 2003, *Planet. Space Sci.*, **51**, 9
- Smith, N. S., Bénilan, Y., & Bruston, P. 1998, *Planet. Space Sci.*, **46**, 1215
- Sylvestre, M., Teanby, N. A., Vinatier, S., Lebonnois, S., & Irwin, P. G. J. 2018, *A&A*, **609**, A64
- Theule, P., Duvernay, F., Ilmane, A., et al. 2011, *A&A*, **530**, A96
- Vila, F., Borowski, P., & Jordan, K. D. 2000, *J. Phys. Chem. A*, **104**, 9009
- Vinatier, S., Bézard, B., Fouchet, T., et al. 2007, *Icarus*, **188**, 120
- Vinatier, S., Bézard, B., Nixon, C. A., et al. 2010, *Icarus*, **205**, 559
- Vinatier, S., Schmitt, B., Bézard, B., et al. 2018, *Icarus*, **310**, 89
- Vuitton, V., Yelle, R., Klippenstein, S., Hörst, S., & Lavvas, P. 2019, *Icarus*, **324**, 120
- Waite, J. H., Young, D. T., Cravens, T. E., et al. 2007, *Science*, **316**, 870
- Wilson, E. H., & Atreya, S. K. 2004, *J. Geophys. Res. Planets*, **109**, E06002
- Zhou, L., Kaiser, R. I., & Tokunaga, A. T. 2009, *Planet. Space Sci.*, **57**, 830